CALCULATION OF SUPERSONIC THREE-DIMENSIONAL FREE-MIXING FLOWS USING THE PARABOLIC-ELLIPTIC NAVIER-STOKES EQUATIONS

By Richard S. Hirsh
NASA Langley Research Center

SUMMARY

A numerical method is presented which is valid for integration of the parabolic-elliptic Navier-Stokes equations. The solution procedure is applied to the three-dimensional supersonic flow of a jet issuing into a supersonic free stream. Difficulties associated with the imposition of free-stream boundary conditions are noted, and a coordinate transformation, which maps the "point at infinity" onto a finite value, is introduced to alleviate these difficulties.

Results are presented for calculations of a square jet and varying-aspect-ratio rectangular jets. The solution behavior varies from axisymmetry for the square jet to nearly two-dimensional for the high-aspect-ratio rectangle, although the computation always calculates the flow as though it were truly three-dimensional.

INTRODUCTION

The calculation of free-mixing flows has, in the past, been accomplished through use of the boundary-layer assumptions in the two-dimensional or axisymmetric Navier-Stokes equations. The accuracy and validity of these procedures have been well documented in the literature (refs. 1 and 2). However, there are numerous situations where the flow cannot be considered either two-dimensional or axisymmetric. Jets issuing from rectangular orifices (see fig. 1), wakes behind any but the simplest bodies, and the flow downstream of a wingtip are examples of three-dimensional free-mixing flows where boundary-layer assumptions are invalid. The characteristic feature of these flows is the importance of diffusion in two spatial coordinates.

These flows have certain characteristics which are common to boundary-layer flows; e.g., the velocities in the planes normal to the main-stream direction are usually much smaller than the main-flow velocity. Consequently, one expects gradients that exist in the cross directions to be larger than the gradients in the main-flow direction. Also, these are usually constant-pressure flows. Therefore, it might be reasonable to

17

use a boundary-layer scaling on the Navier-Stokes equations to effect some simplification; however, this yields an inconsistent set of equations. To lowest order, the cross-stream momentum equations reduce to statements that the pressure is constant, and the resulting number of equations is not sufficient to determine the remaining unknown quantities.

This paper presents the results of a method which overcomes this difficulty and allows numerical solutions of the parabolized Navier-Stokes equations. The method is applied to a three-dimensional, supersonic, rectangular jet problem in which the aspect ratio is varied from one (square jet) to large values representative of slits. The range of applicability of the procedure is demonstrated from the near axisymmetry of the square, through a true three-dimensional region of moderate aspect ratios, to a quasi-two-dimensional flow in the high-aspect-ratio limit which approximates a two-dimensional jet.

SYMBOLS

A,B   transformation constants

$[A],[B],[C]$ matrices defined by equation (15)

$\vec{D}$ vector defined by equation (15)

$\dfrac{D}{Dt}$ convective derivative

h   half-width of unit jet (reference length)

M   Mach number

N_{Pr} Prandtl number

p   pressure

R   Reynolds number

S $= S^*/T_r$

S^* Sutherland's constant

T	temperature
U	velocity
u,v,w	component velocities in x-, y-, and z-directions, respectively
x,y,z	coordinate directions
$\Delta x, \Delta y, \Delta z$	grid spacings in x-, y-, and z-directions, respectively
$\bar{\bar{W}}$	vector of dependent variables (see eq. (16))
γ	ratio of specific heats
Δ	dilatation
δ	central difference operator
η, ζ	transformed y- and z-coordinates
μ	viscosity
ρ	density
Φ	dissipation

Subscripts:

j,k	discretized y- and z-positions, respectively
r	reference quantity
∞	free stream
$+,-$	upper and lower grid spacings used with nonuniform grid

Superscripts:

i	discretized x-position

GOVERNING EQUATIONS

Derivation of Equations

The full three-dimensional Navier-Stokes equations are elliptic in character. The core storage available on present computers is insufficient to practicably handle any but the coarsest computational grids. Thus, methods to reduce the equations to a form more tractable for computation must be employed. A true boundary-layer scaling cannot be used since it yields an inconsistent set of equations; however, some of the concepts from boundary-layer theory indicate the means to simplify the equations.

The only assumption which can be made is the predominance of the convection in one main-flow direction. This leads to the (Reynolds number dependent) conclusion that diffusion can be neglected in this direction when compared with convection. Assuming the x-direction to be the convective direction, the Navier-Stokes equations become

for x-momentum:

$$\rho \frac{Du}{Dt} = -\frac{\partial p}{\partial x} + \left\{ \frac{\partial}{\partial x}\left[\mu\left(2\frac{\partial u}{\partial x} - \frac{2}{3}\Delta\right)\right] \right\} + \frac{\partial}{\partial y}\left[\mu\left(\frac{\partial u}{\partial y}\right)\right] + \frac{\partial}{\partial z}\left[\mu\left(\frac{\partial u}{\partial z}\right)\right] \tag{1}$$

for y-momentum:

$$\rho \frac{Dv}{Dt} = -\frac{\partial p}{\partial y} + \left\{ \frac{\partial}{\partial x}\left[\mu\left(\frac{\partial v}{\partial x}\right)\right] \right\} + \frac{\partial}{\partial y}\left[\mu\left(2\frac{\partial v}{\partial y} - \frac{2}{3}\Delta\right)\right] + \frac{\partial}{\partial z}\left[\mu\left(\frac{\partial v}{\partial z}\right)\right] \tag{2}$$

for z-momentum:

$$\rho \frac{Dw}{Dt} = -\frac{\partial p}{\partial z} + \left\{ \frac{\partial}{\partial x}\left[\mu\left(\frac{\partial w}{\partial x}\right)\right] \right\} + \frac{\partial}{\partial y}\left[\mu\left(\frac{\partial w}{\partial y}\right)\right] + \frac{\partial}{\partial z}\left[\mu\left(2\frac{\partial w}{\partial z} - \Delta\right)\right] \tag{3}$$

where the terms in braces are the streamwise x-direction diffusion terms to be neglected. In addition, since the expression

$$\Delta = \frac{\partial u}{\partial x} + \frac{\partial v}{\partial y} + \frac{\partial w}{\partial z}$$

also introduces x-diffusion terms in the y- and z-crossflow momentum equations, these derivatives are also neglected here. The x-momentum equation is the same as would have been produced by a true boundary-layer scaling, but since no quantitative assumptions have been made concerning the relative sizes of the x-, y-, or z-gradients, the y- and z-momentum equations are retained, although in somewhat simpler form.

The energy equation becomes

$$\rho \frac{DT}{Dt} = \frac{Dp}{Dt} + \frac{1}{N_{Pr}} \left(\left\{ \frac{\partial}{\partial x} \left[\mu \left(\frac{\partial T}{\partial x} \right) \right] \right\} + \frac{\partial}{\partial y} \left[\mu \left(\frac{\partial T}{\partial y} \right) \right] + \frac{\partial}{\partial z} \left[\mu \left(\frac{\partial T}{\partial z} \right) \right] \right) + \mu \Phi \qquad (4)$$

where the term in braces is to be neglected,

$$\Phi = \left(\frac{\partial u}{\partial y} \right)^2 + \left(\frac{\partial u}{\partial z} \right)^2 + \frac{4}{3} \left[\left(\frac{\partial v}{\partial y} \right)^2 - \left(\frac{\partial v}{\partial y} \right) \left(\frac{\partial w}{\partial z} \right) + \left(\frac{\partial w}{\partial z} \right)^2 \right] + \left(\frac{\partial w}{\partial y} \right)^2 - 2 \left(\frac{\partial w}{\partial y} \right) \left(\frac{\partial v}{\partial z} \right) + \left(\frac{\partial v}{\partial z} \right)^2$$

and the convective derivative $\frac{D}{Dt}$ is given by

$$\frac{D}{Dt} = u \frac{\partial}{\partial x} + v \frac{\partial}{\partial y} + w \frac{\partial}{\partial z}$$

All x-gradients in the dissipation have also been neglected. Finally, the continuity equation remains unchanged:

$$\frac{\partial}{\partial x}(\rho u) + \frac{\partial}{\partial y}(\rho v) + \frac{\partial}{\partial z}(\rho w) = 0 \qquad (5)$$

When these equations are supplemented by an equation of state and a viscosity relation,

$$p = \rho RT \qquad (6a)$$

$$\frac{\mu}{\mu_r} = \left(\frac{T_r + S^*}{T + S^*} \right) \left(\frac{T}{T_r} \right)^{3/2} \qquad (6b)$$

where R is the universal gas constant, a system of five equations for five unknowns is obtained after elimination of the density by the perfect gas equation of state.

The elliptic nature of the Navier-Stokes equations in the x-direction has thus been eliminated; consequently, the equations are parabolic in x and marching integration may be used in the streamwise direction. This is significant computationally since it eliminates the need to store all the field quantities at each x-location which results in a substantial reduction in computer storage. Thus, the name parabolic-elliptic Navier-Stokes equations, since the assumptions allow a march in x away from an initial data plane, yet retain the elliptic character of the crossflow planes (Y-Z planes) due to the inclusion of all second derivatives in y and z. Flows with swirl or possible cross-flow recirculation (vortices) in the Y-Z planes can be computed, and only reverse flow in the main-stream direction is eliminated due to the omission of x-diffusion.

It should be noted that the continuity equation is hyperbolic; however, a march in the streamwise direction is still possible since the x-derivative can be expanded as follows:

$$(\rho u)_x = \left(\frac{pu}{T}\right)_x = \frac{u}{T}\, p_x + \frac{p}{T}\, u_x - \frac{pu}{T^2}\, T_x$$

and the p_x term can be used to advance to the next station. There is no explicit diffusion term present and discontinuities which may be present can be expected to persist for large x-distances; hence, smooth initial profiles are desirable.

Equations similar to these have recently been used for supersonic flow past a sharp cone at incidence (ref. 3) and for hypersonic leading-edge flows, where a more formal analysis and scaling can be invoked (ref. 4). To date, no detailed work has been published on three-dimensional free-mixing flows.

Validity for Supersonic Jet Flows

Free jet and wake flows are common aerodynamic phenomena. These flows are generally turbulent, and the calculation of two-dimensional or axisymmetric turbulent free jets or wakes is difficult (ref. 2) because of problems associated with turbulence modeling; higher order modeling (two-equation models) is necessary in many cases. For three-dimensional flows with two essential cross-plane velocities, very few calculations have been made. To assess the modeling procedures for a three-dimensional flow, a calculation procedure valid for laminar flows, preferably in primitive variables to allow ease of incorporation of the turbulence models, is required. The parabolic-elliptic equations (eqs. (1) to (6)) need to be verified for laminar jet calculations prior to their application to turbulent flows.

If the equations are cast in nondimensional form by using free-stream values of U_∞, p_∞, and T_∞ and some suitable reference length which characterizes the problem, the equations become

for x-momentum:

$$\rho\frac{Du}{Dt} = -\frac{1}{\gamma M_\infty^2}\frac{\partial p}{\partial x} + \frac{1}{R}\left\{\frac{\partial}{\partial y}\left[\mu\left(\frac{\partial u}{\partial y}\right)\right] + \frac{\partial}{\partial z}\left[\mu\left(\frac{\partial u}{\partial z}\right)\right]\right\} \tag{7}$$

for y-momentum:

$$\rho\frac{Dv}{Dt} = -\frac{1}{\gamma M_\infty^2}\frac{\partial p}{\partial y} + \frac{1}{R}\left\{\frac{\partial}{\partial y}\left[\mu\left(2\frac{\partial v}{\partial y} - \frac{2}{3}\Delta\right)\right] + \frac{\partial}{\partial z}\left[\mu\left(\frac{\partial v}{\partial z}\right)\right]\right\} \tag{8}$$

for z-momentum:

$$\rho\frac{Dw}{Dt} = -\frac{1}{\gamma M_\infty^2}\frac{\partial p}{\partial z} + \frac{1}{R}\left\{\frac{\partial}{\partial y}\left[\mu\left(\frac{\partial w}{\partial y}\right)\right] + \frac{\partial}{\partial z}\left[\mu\left(2\frac{\partial w}{\partial z} - \frac{2}{3}\Delta\right)\right]\right\} \tag{9}$$

for energy:

$$\rho \frac{DT}{Dt} = \left(\frac{\gamma - 1}{\gamma}\right)\frac{Dp}{Dt} + \frac{1}{N_{Pr}R}\left\{\frac{\partial}{\partial y}\left[\mu\left(\frac{\partial T}{\partial y}\right)\right] + \frac{\partial}{\partial z}\left[\mu\left(\frac{\partial T}{\partial z}\right)\right]\right\} + \frac{\gamma - 1}{R}M_\infty^2\mu\left\{\left(\frac{\partial u}{\partial y}\right)^2 + \left(\frac{\partial u}{\partial z}\right)^2\right.$$

$$\left. + \frac{4}{3}\left[\left(\frac{\partial v}{\partial y}\right)^2 - \left(\frac{\partial v}{\partial y}\right)\left(\frac{\partial w}{\partial z}\right) + \left(\frac{\partial w}{\partial z}\right)^2\right] + \left(\frac{\partial w}{\partial y}\right)^2 - 2\left(\frac{\partial w}{\partial y}\right)\left(\frac{\partial v}{\partial z}\right) + \left(\frac{\partial v}{\partial z}\right)^2\right\} \tag{10}$$

for continuity:

$$\frac{\partial}{\partial x}(\rho u) + \frac{\partial}{\partial y}(\rho v) + \frac{\partial}{\partial z}(\rho w) = 0 \tag{11}$$

and for Sutherland's law:

$$\mu = \left(\frac{1 + S}{T + S}\right)T^{3/2} \tag{12}$$

Rubin and Lin (ref. 5) have shown that equations of this type are singular at $M = 1$ if the p_x term is treated exactly and singular at $M = 0$ if the p_x term is calculated in an explicit manner during the numerical calculation. If the p_x term is neglected entirely or specified from a boundary-layer approximation, then the parabolic march in x can proceed without difficulty. Thus, it was felt that since the p_x term should be included if necessary, the problem chosen to test the overall method should avoid any of these obvious integration difficulties. The $M = 0$ behavior takes place near boundaries (where $u = 0$), and therefore, the free jet problem avoids this singular behavior. However, the jet cannot exhaust into an ambient atmosphere since here too $u = 0$. Thus a jet issuing into a moving free stream is suitable. To avoid any difficulties at $M = 1$ both streams were chosen to be supersonic. Thus, equations (7) to (12) will be solved for a supersonic jet issuing into a supersonic free stream.

NUMERICAL PROCEDURE

Integration Technique

An implicit numerical procedure was chosen to solve the governing equations for a number of reasons. The success of implicit methods on the two- and three-dimensional boundary-layer equations implies that they should be efficient for the boundary-layer-like parabolic-elliptic Navier-Stokes equations (eqs. (7) to (12)). It is expected that solutions will be required at large distances downstream from the initial data plane; consequently, large x-steps are desirable. The need to eliminate the step size restrictions of explicit methods leads to a consideration of unconditionally stable methods which are consistent in their marching variation. The particular implicit method used in this study is the alternating-direction implicit (ADI) method of Peaceman and Rachford (ref. 6). The

ADI method is ideally suited for the solution of equations (7) to (12). There is no stability restriction on the step size, and hence, large x-steps are permitted. The method has second-order truncation error in its marching variation, which is also a requirement for the type of flow envisioned, since the x-history of the flow must be traced accurately at each step. Finally, the method does not require the inversion of a sparse-banded matrix, as a fully implicit or Crank-Nicolson method would. Simple tridiagonal coefficient matrices are generated at each step which require much less storage and time for their inversion in relation to sparse-banded matrices. The method has previously been shown to be effective for a set of equations similar to those used in the present approach (ref. 7).

The ADI procedure is used to difference in x, with the y- and z-derivatives expressed as central differences, with the option of a nonuniform grid included; that is,

$$\delta_z u^i_{j,k} = \frac{\partial u}{\partial z} = \frac{(\Delta z_-)^2 u^i_{j,k+1} - \left[(\Delta z_+)^2 - (\Delta z_-)^2\right] u^i_{j,k} - (\Delta z_+)^2 u^i_{j,k-1}}{(\Delta z_+)(\Delta z_-)\left[(\Delta z_+) + (\Delta z_-)\right]}$$

$$\delta_z^2 u^i_{j,k} = \frac{\partial^2 u}{\partial z^2} = 2\left\{\frac{(\Delta z_-) u^i_{j,k+1} - \left[(\Delta z_+) + (\Delta z_-)\right] u^i_{j,k} + (\Delta z_+) u^i_{j,k-1}}{(\Delta z_+)(\Delta z_-)\left[(\Delta z_+) + (\Delta z_-)\right]}\right\}$$

An example of the complete differencing scheme is shown for the x-momentum equation as follows:

$$(\rho u)^{i+\frac{1}{2}}_{j,k}\left(\frac{u^*_{j,k} - u^i_{j,k}}{\Delta x/2}\right) + (\rho v)^{i+\frac{1}{2}}_{j,k}\delta_y u^i_{j,k} + (\rho w)^{i+\frac{1}{2}}_{j,k}\delta_z u^*_{j,k} = -\frac{1}{\gamma M_\infty^2}\left(\frac{p^*_{j,k} - p^i_{j,k}}{\Delta x/2}\right)$$

$$+ \frac{1}{R}\left\{\frac{1}{2}\left(\frac{\partial \mu}{\partial T}\right)^{i+\frac{1}{2}}_{j,k}\left[\left(\frac{\partial T}{\partial y}\right)^{i+\frac{1}{2}}_{j,k}\delta_y u^i_{j,k} + \left(\frac{\partial u}{\partial y}\right)^{i+\frac{1}{2}}_{j,k}\delta_y T^i_{j,k}\right] + \mu^{i+\frac{1}{2}}_{j,k}\delta_y^2 u^i_{j,k} + \frac{1}{2}\left(\frac{\partial \mu}{\partial T}\right)^{i+\frac{1}{2}}_{j,k}\left[\left(\frac{\partial T}{\partial z}\right)^{i+\frac{1}{2}}_{j,k}\delta_z u^*_{j,k}\right.$$

$$\left. + \left(\frac{\partial u}{\partial z}\right)^{i+\frac{1}{2}}_{j,k}\delta_z T^*_{j,k}\right] + \mu^{i+\frac{1}{2}}_{j,k}\delta_z^2 u^*_{j,k}\right\} \tag{13a}$$

$$(\rho u)_{j,k}^{i+\frac{1}{2}}\left(\frac{u_{j,k}^{i+1} - u_{j,k}^*}{\Delta x/2}\right) + (\rho v)_{j,k}^{i+\frac{1}{2}}\delta_y u_{j,k}^{i+1} + (\rho w)_{j,k}^{i+\frac{1}{2}}\delta_z u_{j,k}^* = -\frac{1}{\gamma M_\infty^2}\left(\frac{p_{j,k}^{i+1} - p_{j,k}^*}{\Delta x/2}\right)$$

$$+\frac{1}{R}\left\{\frac{1}{2}\left(\frac{\partial\mu}{\partial T}\right)_{j,k}^{i+\frac{1}{2}}\left[\left(\frac{\partial T}{\partial y}\right)_{j,k}^{i+\frac{1}{2}}\delta_y u_{j,k}^{i+1} + \left(\frac{\partial u}{\partial y}\right)_{j,k}^{i+\frac{1}{2}}\delta_y T_{j,k}^{i+1}\right] + \mu_{j,k}^{i+\frac{1}{2}}\delta_y{}^2 u_{j,k}^{i+1} + \frac{1}{2}\left(\frac{\partial\mu}{\partial T}\right)_{j,k}^{i+\frac{1}{2}}\left[\left(\frac{\partial T}{\partial z}\right)_{j,k}^{i+\frac{1}{2}}\delta_z u_{j,k}^*\right.$$

$$\left.+ \left(\frac{\partial u}{\partial z}\right)_{j,k}^{i+\frac{1}{2}}\delta_z T_{j,k}^*\right] + \mu_{j,k}^{i+\frac{1}{2}}\delta_z{}^2 u_{j,k}^*\right\} \tag{13b}$$

The only difficulty arises from the cross derivatives of velocity present in the y- and z-momentum equations. These cannot be differenced implicitly since the tridiagonal structure of the resulting matrices would be destroyed. These are treated in the same manner as all the nonlinear coefficients present in the differenced equations.

Linearization Scheme

The ADI procedure, which is second-order accurate, centers the x-derivatives about the point $\left(i + \frac{1}{2}\right)$. (See fig. 2.) This point is not equivalent to the intermediate step of the ADI procedure. Hence, a method must be developed to compute all the nonlinear coefficients (and the cross derivatives) at the $\left(i + \frac{1}{2}\right)$ point. This can be accomplished by a quadratic extrapolation from the two previous x-stations (i) and (i - 1) (ref. 7) or by use of the predictor-corrector procedure of Douglas and Jones (ref. 8). Both of these require additional storage. The procedure used in the present work handles the nonlinear terms by an iterative technique similar to that used for boundary-layer calculations in which a Crank-Nicolson integration is used (ref. 9). Any coefficient Q is calculated at the mid-point $\left(i + \frac{1}{2}\right)$ by the simple formula

$$Q_{j,k}^{i+\frac{1}{2}} = \frac{1}{2}\left(Q_{j,k}^{i+1} + Q_{j,k}^i\right) \tag{14}$$

The value at (i + 1) is not known on the first iteration and so the Q^i value is used. After the integration to (i + 1) has been completed, new values of Q^{i+1} are computed, and the integration step to (i + 1) is repeated to either a specified convergence or a specified number of iterations. At convergence this yields second-order-accurate coefficients which match the accuracy of the integration. The cross derivatives are also treated this way.

The resulting linear difference equations are a set of five equations in five unknowns. Rather than make the quite arbitrary choice of the order of solution if a sequential technique of solving each equation in turn were elected, the five equations are solved simultaneously. The resulting matrix equation has a block tridiagonal structure which can be represented as

$$\left[A_j\right]\vec{W}_{j+1} + \left[B_j\right]\vec{W}_j + \left[C_j\right]\vec{W}_{j-1} = \vec{D}_j \tag{15}$$

where the unknown vector $\vec{W}_j$ contains all the five unknowns

$$\vec{W}_j = \left(u_j, v_j, w_j, T_j, p_j\right)^T \tag{16}$$

the coefficients $\left[A\right]$, $\left[B\right]$, and $\left[C\right]$ are simply the matrix coefficients of each particular unknown; that is,

$$\left[A_j\right] \approx \begin{pmatrix} a_{11j} & a_{12j} & \cdot & \cdot & \cdot & a_{15j} \\ a_{21j} & & & & & \cdot \\ \cdot & & & & & \cdot \\ \cdot & & & & & \cdot \\ \cdot & & & & & \cdot \\ a_{51j} & \cdot & \cdot & \cdot & \cdot & a_{55j} \end{pmatrix} \tag{17}$$

and the vector $\vec{D}$ is a source term in each equation. The components a_{mnj} represent the coefficient of the nth unknown from the mth equation at point j.

The inversion of this block matrix is particularly simple. It consists of rewriting the usual tridiagonal algorithm with all multiplications replaced by matrix multiples, and all divisions replaced by matrix inversions. This simultaneous solution procedure was used previously by Krause, Hirschel, and Bothmann (ref. 9) where the pressure, of course, was not one of the unknown variables due to the boundary-layer assumptions. The procedure is quite advantageous because, in addition to eliminating the previously mentioned choice of solution order, it models the physics more precisely by allowing changes in any variable to be instantaneously sensed by all the others. It is also believed that this procedure aids in the convergence of the iteration since it eliminates the use of lagged information previously calculated in a sequential solution. Thus it is fully implicit in the sense that a sequential solution is much like a Gauss-Seidel iteration which is explicit.

The number of grid points used for the calculation was governed by conflicting requirements. For acceptable resolution, many points were desirable in the shear layer

between the jet and free stream and in the jet itself. Also, reasonable distances away from the high shear region were necessary to allow boundary conditions in the free stream to be applied without distorting the results interior to the computational domain. However, excessive mesh points result in unacceptable machine storage requirements, increase computational time extravagantly, and impair job turnaround time. An initial compromise was to use a 41 × 41 grid to compute the quarter-plane of the jet flow, using the symmetry axes of the jet as boundaries. An equally spaced grid of $\Delta y = \Delta z = 0.1$ was first utilized, thereby placing a jet half-width at five grid spacings away from the axis and the outer edge of the domain seven times beyond this (40 grid spacings away from the axis). The required computer storage was $130\ 000_8$ on the CDC 6600 system.

Initial Conditions

The initial conditions at the data plane representing the orifice location $x = 0$ were chosen in a very rudimentary manner. Since too many points would be necessary to describe the merging of the free stream and duct flows just past a jet exit, and storage limitations were severe enough before this consideration, the initial velocity profiles were chosen as shown in figure 3. The jet and free stream are represented by two distinct inviscid flows separated by a sharp boundary. Computationally this yields a one-grid-point discontinuity between u_{jet} and U_∞. This initial condition is probably the most severe that can be imposed while still generating an eventually realistic flow description. The initial conditions on the crossflow velocities were also modeled simply and were set equal to zero.

The pressure distribution was chosen to be uniform at the free-stream level since an unmatched static pressure would undoubtedly produce shocks. These were not consciously sought as part of the problem, and the initial conditions were set to try to avoid their generation. The streamwise velocity and temperature levels were computed by assuming constant total temperature in the jet and free stream and specifying the jet and free-stream Mach numbers.

The free jet problem was expected to encounter few boundary condition troubles due to the avoidance of all $u = 0$ boundary conditions. The conditions placed on the variables were symmetry with no crossflow on the axes of the jet and consistent free-stream conditions. Difficulties encountered with the application of these conditions are discussed in the next section.

RESULTS AND DISCUSSION

A standard test case was chosen to check the numerical procedure: the free-stream Mach number was set equal to 5.0; the jet Mach number at the initial station was 7.5. The reference length was set equal to the minimum initial orifice width of a

1×1 square jet. The Reynolds number based on this reference length was set equal to 10^3, and the Prandtl number was set equal to 1.

Effect of Initial Conditions

The initial behavior (small x) for all cases computed regardless of the grid configuration or boundary conditions applied was essentially the same. The discontinuous velocity and temperature profiles were smoothed out by the diffusive terms, but the continuity equation reacted to these discontinuities differently. The initial and subsequent u, T, and p profiles are shown qualitatively in figure 4. Referring to the figure, in the region below the initial discontinuity, $u_x < 0$ and $T_x > 0$, and above, $u_x > 0$ and $T_x < 0$. The x-gradients in the continuity equation appear as follows:

$$\frac{p}{T} \frac{\partial u}{\partial x} - \frac{pu}{T^2} \frac{\partial T}{\partial x} + (y \text{ and } z \text{ gradients}) = -\frac{u}{T} \frac{\partial p}{\partial x} \tag{18}$$

Above the original discontinuity then, $p_x < 0$, and below, $p_x > 0$, neglecting the y- and z-gradients which are smaller here than the x-gradients. Hence, the pressure develops a blip around the initial discontinuity (see fig. 4) which persists for some distance before the profiles lose the influence of the initial conditions. This high-pressure-gradient profile causes divergence of the normal velocities about the initial breakpoint until the entrainment-induced boundary-layer-like velocities away from the jet axis are established. Eventually the pressure profiles smooth out to the expected constant case, but since the continuity equation is hyperbolic and contains no damping, ripples in the pressure profile of 0.2 percent of the free stream are commonplace. However, this initial behavior is of no concern, except in its influence on the downstream results, since the parabolic approximation is not valid in this region of very high x-gradients.

Since the pressure is expected to be approximately constant in the developed jet, an attempt to artificially drive the pressure to its constant value more quickly was made. An artificial diffusion term was introduced into the continuity equation in the hope of quickly smoothing the pressure profile. However, it was found that any introduction of these terms generated more diffusion in the other variables as well. Only values of an artificial viscosity larger than the actual flow viscosity had any significant effect and no improvement was effected by the incorporation of these fictitious terms. Thus, the flow was permitted to naturally adjust to the initial discontinuity. If this was smoothed initially over a few grid points, the pressure disturbance was smaller and shorter lived. Consequently it appears that no difficulties will be encountered if correct initial data are prescribed from experiments or boundary-layer calculations.

Problems Associated With Application of Boundary Conditions

The expectation that the elimination of solid walls and stagnant regions would ease boundary condition difficulties was not realized. The boundaries of the computational domain were the axes of symmetry of the jet and the point in the free stream considered to approximate infinity. The conditions to be applied at these axes were symmetry of all quantities except the cross-plane velocity normal to the axis which was equal to zero. Thus at $y = 0$, for example, the conditions to be applied were $u_y = w_y = T_y = p_y = 0$ and $v = 0$. Writing the governing equations differenced on the boundary (see fig. 5) and using the above relations to eliminate the unknown points outside the domain created by the central differences resulted in the values of the functions on the boundary becoming an additional row of unknowns to the vector $\overline{W}_j$ in the block tridiagonal system. The inversion technique thus allowed the simultaneous solution of the boundary values as well as the interior points, and the resulting solution was smooth for all variables except the pressure. At the symmetry plane the pressure profile contained a spike (see fig. 6) and the other unknowns had gradients which differed from zero. This entire difficulty was eliminated by imposing a quadratic fit for the zero gradient condition onto each of the variables. The relation

$$u_1 = \frac{4u_2 - u_3}{3} \tag{19}$$

insures a zero gradient with second-order accuracy, which matches the truncation of the difference scheme, and retains the tridiagonal aspect of the solution matrices.

The "infinity" boundary conditions must be imposed at boundaries in the free stream. These boundary conditions could be imposed at a suitable distance from the symmetry plane if asymptotic conditions could be derived far from the jet. However, asymptotic conditions are not known for the three-dimensional jet, and even if they were, the question arises as to a suitable distance at which they could be applied. Treatment of these boundary conditions can be classified into two groups: alterations in the actual conditions imposed at the last grid point and, concurrent with these, changes in the grid size.

At first, all variables were specified at their free-stream values; that is, $u = T = p = 1$ and $v = w = 0$ at the last grid point in the domain with a uniform grid. The calculation proceeded smoothly, but after the usual jet crossflow velocity established itself, a sharp, one-grid-width gradient developed at the outer edge of the computational domain due to the difference between the negative entrainment velocity and the imposed zero value. (See fig. 7.). To alleviate this condition, an expanding nonuniform grid was used in place of the uniform one. Where the uniform 41×41 grid had $y = z = 4$ as the last grid point, the nonuniform grid using the same number of points allowed the edge to be displaced to $y = z = 17.5$, after remaining uniform to $y = z = 1$. This resulted in a

delay in the appearance of this boundary gradient until the solution marched further downstream; however, it did not eliminate the problem.

The expanding jet both deflects the crossflow away from the jet axes and entrains fluid from the free stream. An interaction between the jet and variables such as v, w, and possibly p is quite likely to be present, and consequently, the specification of values for these quantities at some finite near point would be of doubtful validity. Instead, the equations should determine the necessary boundary effects. To do this, a quadratic extrapolation consistent with the second-order differencing was imposed on v, w, and p by using both the uniform and nonuniform grids. The pressure solution quickly deteriorated and the cause was traced to the lack of actual specification of a pressure level. With zero gradient conditions on the axes and extrapolation at the outer edge, no fixed pressure value is specified. Hence, the extrapolation was limited to the crossflow velocities, which proved more successful, and the x-marching proceeded to a distance of approximately 20 jet widths. However, difficulties again occurred at the outer edge of the domain as shown in figure 8. The expected crossflow velocities appeared and the extrapolation did not affect the profiles. But, as the jet proceeds downstream, it grows and the zero velocity point of the crossflow moves out from the axes. Eventually, as shown in figure 8, this point moved completely out of the computational domain, leaving only outflow from the centerline which is not characteristic of a jet.

Until this point was reached, the development of the profiles showed the correct trend for the streamwise velocity (see fig. 9) but, as later calculations indicated, the greatest x-distance achieved was well ahead of the end of the jet core region, even if the nonuniform grid was used. For the square jet initial profile, all the variables were computed symmetrically about the jet axis, and the pressure became uniform to within 0.2 percent of the free-stream value.

All these difficulties with edge conditions arise due to the growth of the jet with x when it is computed by using the unscaled spatial coordinates. To overcome this problem area a transformation was introduced in the Y-Z plane to contain the jet totally within the computational domain.

Transformation of Coordinates

The objective in transforming the coordinates is to aid in the imposition of "infinity" boundary conditions. The uncertainty in these conditions can be overcome only if the exact free-stream conditions can be imposed. To enable this to be accomplished, the point at infinity must be mapped to a finite point in the transformed space. One of the simpler transformations by which this can be accomplished is

$$\eta = \frac{Ay}{1 + Ay} \tag{20a}$$

$$\zeta = \frac{Bz}{1 + Bz} \tag{20b}$$

which maps zero onto zero and infinity in the physical plane onto unity in the η-ζ plane. With equations (20) the governing equations are as follows (with $\xi = x$):

$$\rho u u_\xi + \left[\rho v + 2A\mu(1 - \eta)\right]A(1 - \eta)^2 u_\eta + \left[\rho w + 2B\mu(1 - \zeta)\right]B(1 - \zeta)^2 u_\zeta = -\frac{1}{\gamma M_\infty^2} p_\xi$$

$$+ \frac{1}{R}\left[A^2(1 - \eta)^4\left(\mu_T T_\eta u_\eta + u_{\eta\eta}\right) + B^2(1 - \zeta)^2\left(\mu_T T_\zeta u_\zeta + u_{\zeta\zeta}\right)\right] \tag{21}$$

$$\rho u v_\xi + \left[\rho v + \frac{8}{3}A\mu(1 - \eta)\right]A(1 - \eta)^2 v_\eta + \left[\rho w + 2B\mu(1 - \zeta)\right]B(1 - \zeta)^2 v_\zeta = -\frac{1}{\gamma M_\infty^2}A(1 - \eta)^2 p_\eta$$

$$+ \frac{1}{R}\left\{\frac{4}{3}A^2(1 - \eta)^4\left(\mu_T T_\eta v_\eta + \mu v_{\eta\eta}\right) + B^2(1 - \zeta)^4\left(\mu_T T_\zeta v_\zeta + \mu v_{\zeta\zeta}\right)\right.$$

$$\left. + AB(1 - \eta)^2(1 - \zeta)^2\left[\frac{1}{3}\mu w_{\eta\zeta} + \mu_T\left(T_\zeta w_\eta - \frac{2}{3}T_\eta w_\zeta\right)\right]\right\} \tag{22}$$

$$\rho u w_\xi + \left[\rho v + 2A\mu(1 - \eta)\right]A(1 - \eta)^2 w_\eta + \left[\rho w + \frac{8}{3}B\mu(1 - \zeta)\right]B(1 - \zeta)^2 w_\zeta = -\frac{1}{\gamma M_\infty^2}B(1 - \zeta)^2 p_\zeta$$

$$+ \frac{1}{R}\left\{A^2(1 - \eta)^4\left(\mu_T T_\eta w_\eta + \mu w_{\eta\eta}\right) + \frac{4}{3}B^2(1 - \zeta)^4\left(\mu_T T_\zeta w_\zeta + \mu w_{\zeta\zeta}\right)\right.$$

$$\left. + AB(1 - \eta)^2(1 - \zeta)^2\left[\frac{1}{3}\mu v_{\eta\zeta} + \mu_T\left(T_\eta v_\zeta - \frac{2}{3}T_\zeta v_\eta\right)\right]\right\} \tag{23}$$

$$\rho u T_\xi + \left[\rho v + \frac{2\mu}{N_{Pr}}A(1 - \eta)\right]A(1 - \eta)^2 T_\eta + \left[\rho w + \frac{2\mu}{N_{Pr}}B(1 - \zeta)^2\right]B(1 - \zeta)^2 T_\zeta = \frac{\gamma - 1}{\gamma}\left[u p_\xi\right.$$

$$+ vA(1 - \eta)^2 p_\eta + wB(1 - \zeta)^2 p_\zeta\right] + \frac{1}{N_{Pr}R}\left[A^2(1 - \eta)^4\left(\mu_T T_\eta^2 + \mu T_{\eta\eta}\right) + B^2(1 - \zeta)^4\left(\mu_T T_\zeta^2\right.\right.$$

$$\left.\left. + \mu T_{\zeta\zeta}\right)\right] + \frac{(\gamma - 1)M_\infty^2}{R}\mu\left[A^2(1 - \eta)^4\left(u_\eta^2 + w_\eta^2 + \frac{4}{3}v_\eta^2\right) + B^2(1 - \zeta)^4\left(u_\zeta^2 + v_\zeta^2 + \frac{4}{3}w_\zeta^2\right)\right.$$

$$\left. + AB(1 - \eta)^2(1 - \zeta)^2\left(w_\eta v_\zeta - \frac{4}{3}v_\eta w_\zeta\right)\right] \tag{24}$$

557

$$up_\xi - \rho u T_\xi + pu_\xi + A(1-\eta)^2\left(vp_\eta - \rho v T_\eta + pv_\eta\right) + B(1-\zeta)^2\left(wp_\zeta - \rho w T_\zeta + pw_\zeta\right) = 0 \qquad (25)$$

These equations were cast in finite difference form and solved numerically by using the same ADI method, linearization scheme, and block tridiagonal solution algorithm as previously discussed. The boundary conditions $u = T = p = 1$ and $v = w = 0$ are imposed at $\eta = 1$ or $\zeta = 1$, corresponding to infinity in the untransformed plane. A coarse 21×21 equally spaced mesh was used on the unit square in the η-ζ plane to reduce the core storage to more acceptable levels (63000_8) for computation.

Results Computed in Transformed Plane

Cases comparable to the ones calculated on the untransformed variables were computed successfully for a variety of initial geometries with no difficulty. The loss of entrainment velocities never occurred, confirming the usefulness of the transformation.

The first test case was a square jet with unit sides. The streamwise centerline velocity decay of this jet is presented in figure 10. After a lengthy core region the centerline velocity quickly decays according to the laminar relation for axisymmetric jets x^{-1} (ref. 1). Thus, although the equations compute the flow as if it were truly three-dimensional, the axisymmetry is reproduced. Another square jet was computed to test the transformation. A large jet with sides of length equal to four was formed by taking unequal scalings of y and z. That is, five points in ζ sufficed to give $z = 2$ (half the jet width), while 11 points in η were necessary to give the equivalent $y = 2$. The centerline decay for this case is also shown in figure 10. After a much longer core than the 1×1 jet (since the initial shear layer is four times farther from the axis), this configuration also very rapidly begins to decay along the axisymmetric curve. In fact, if the 1×1 curve is displaced to the right by the difference of core lengths, the decay curves coincide.

The three-dimensional capabilities of the method were tested on rectangular jets of varying aspect ratios. A rectangular 2×1 jet gave results for velocity decay shown in figure 10. The initial core region was of the same length as the 1×1 square jet. However, the decay was slower than the 1×1 jet, and in fact there was a region where the two-dimensional laminar jet decay $x^{-1/3}$ described the flow. Eventually though, the decay increased and approached the axisymmetric behavior seen before with slope x^{-1}. Only this far-field behavior could be described by an axisymmetric boundary-layer analysis, whereas the length to its asymptotic decay could not.

A rectangular 4×1 jet is more two-dimensional than either of the previous cases, as indicated by its decay. (See fig. 10.) After the initial core length, characteristic of the distance needed for disturbances one width away from the centerline to reach the axis, the decay curve obviously follows the two-dimensional slope for a greater distance down-

stream to about x = 500 (see fig. 10) where it also gradually starts to approach the axisymmetric curve. The length x = 500 is not too surprising, for this is the core distance of the 4 × 4 square jet, the distance needed for disturbances four widths away to reach the axis. The even higher aspect ratio 8 × 1 jet continued the established trend and is also shown in figure 10.

Finally, note the advantage gained through the use of the transformation. Prior to its use, by using a greatly expanding mesh in the untransformed plane with extrapolation at the last mesh point, complete loss of entrainment took place at approximately x = 20. Even at this point the accuracy of the solution is questionable, and this is not even halfway to the end of the core region as computed by using the transformation and depicted in figure 10.

CONCLUDING REMARKS

The parabolic-elliptic Navier-Stokes equations have been shown to be a viable method for computation of three-dimensional supersonic jet flows. The difficulties associated with the unbounded domain of the jet can be eliminated by incorporating a transformation into the equations so that the points of infinity in the cross plane are mapped to a finite value at the transformed plane.

Although the character of the computed flow can be predominantly axisymmetric in the case of the square jet or approach a two-dimensional limit, as is the case for the 8 × 1 rectangular jet, no prior assumptions to this effect are required. The solution computes the particular flow under investigation as though it were three-dimensional, allowing the initial geometry of the prescribed jet to determine the ultimate nature of the solution.

The present calculations have been for laminar jets; however, jet flows are generally turbulent. Thus, even if some simpler method could be used instead of the present integration scheme to recover the gross characteristic of the laminar flow, the inclusion of turbulence modeling in the fully elliptic crossplane requires numerical treatment.
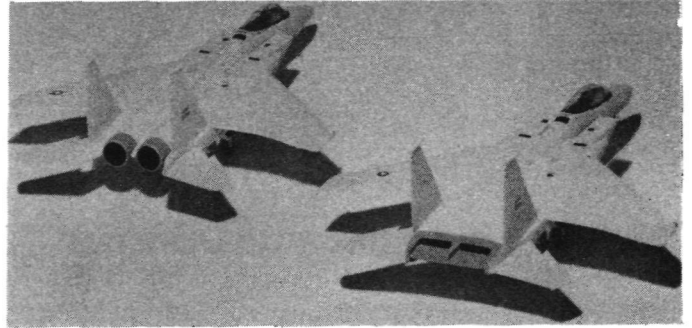
A subsonic analog of the parabolic-elliptic Navier-Stokes equations, where the streamwise pressure gradient is correctly accounted for, is currently being investigated so that the more advanced state of the higher order incompressible turbulence models can be drawn upon for inclusion into the governing equations. If this proves successful, then the supersonic equations will be used as a means to test various modeling procedures for compressible turbulent flows.

REFERENCES

1. Schlichting, Hermann (J. Kestin, transl.): Boundary Layer Theory. Fourth ed., McGraw-Hill Book Co., Inc., c.1960.

2. Free Turbulent Shear Flows. Volume I — Conference Proceedings. NASA SP-321, 1973.

3. Lubard, Stephen C.; and Helliwell, William S.: Calculation of the Flow on a Cone at High Angle of Attack. AIAA Paper No. 73-636, July 1973.

4. Rudman, S.; and Rubin, S. G.: Hypersonic Viscous Flow Over Slender Bodies With Sharp Leading Edges. AIAA J., vol. 6, no. 10, Oct. 1968, pp. 1883-1890.

5. Rubin, S. G.; and Lin, T. C.: Numerical Methods for Two- and Three-Dimensional Viscous Flow Problems: Application to Hypersonic Leading Edge Equations. AFOSR-TR-71-0778, U.S. Air Force, Apr. 1971. (Available from DDC as AD 726 547.)

6. Peaceman, D. W.; and Rachford, H. H., Jr.: The Numerical Solution of Parabolic and Elliptic Differential Equations. J. Soc. Ind. & Appl. Math., vol. 3, no. 1, Mar. 1955, pp. 28-41.

7. Nardo, C. T.; and Cresci, R. J.: An Alternating Directional Implicit Scheme for Three-Dimensional Hypersonic Flows. J. Comput. Phys., vol. 8, no. 2, Oct. 1971, pp. 268-284.

8. Douglas, Jim, Jr.; and Jones, B. F., Jr.: On Predictor-Corrector Methods for Non-linear Parabolic Differential Equations. J. Soc. Ind. & Appl. Math., vol. 11, no. 1, Mar. 1963, pp. 195-204.

9. Krause, E.; Hirschel, E. H.; and Bothmann, Th.: Differenzenformeln zur Berechnung Dreidimensionaler Grenzschichten (Finite Difference Equations for Calculating Three-Dimensional Boundary Layers). DLR FB 69-66, Sept. 1969.
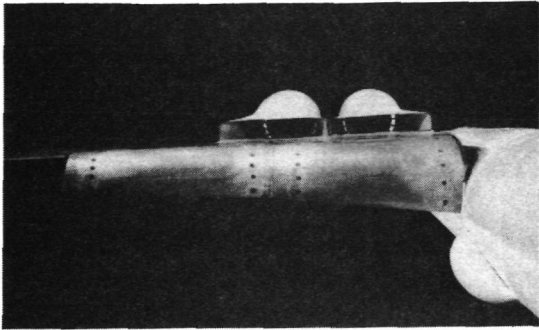
(a) Upper surface blowing.　　　　(b) F-15 with proposed rectangular nozzle.

Figure 1.- Examples of three-dimensional jets in aerodynamic flows.
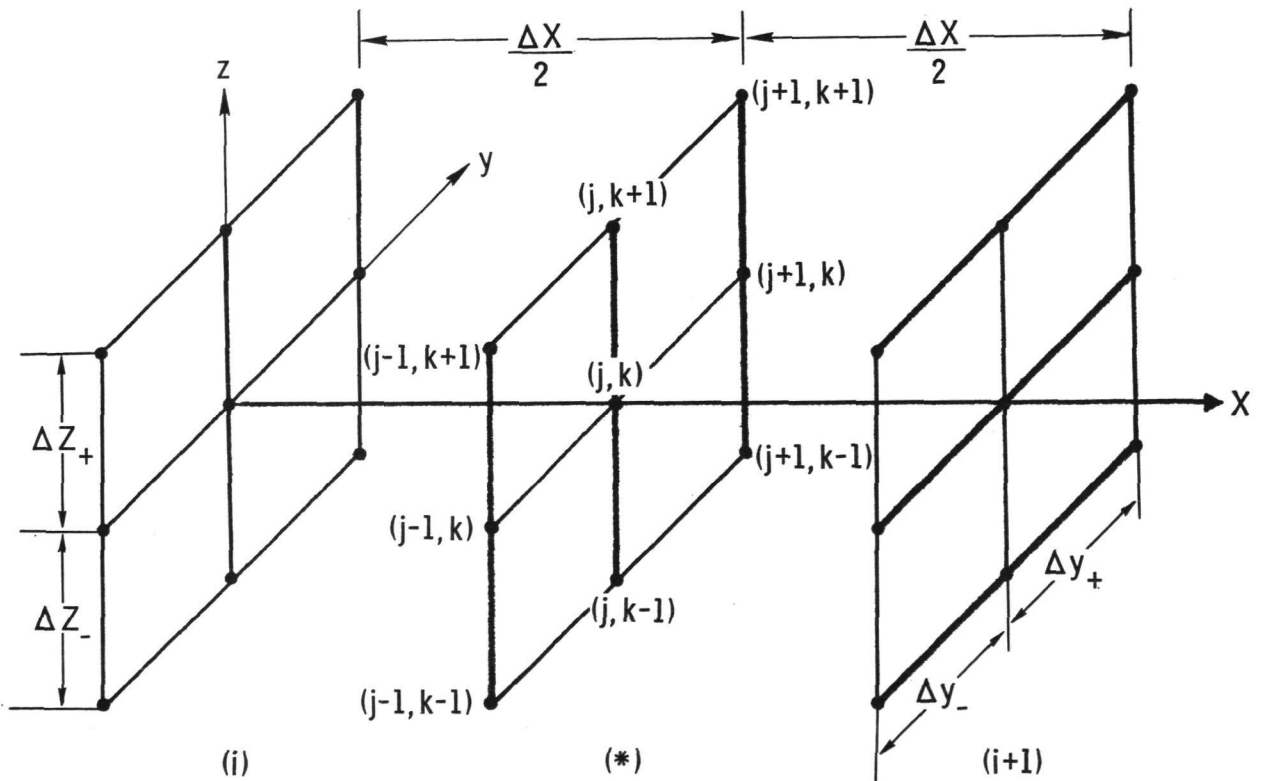
Figure 2.- The ADI procedure: first step implicit in z, explicit in y; second step implicit in y, explicit in z.
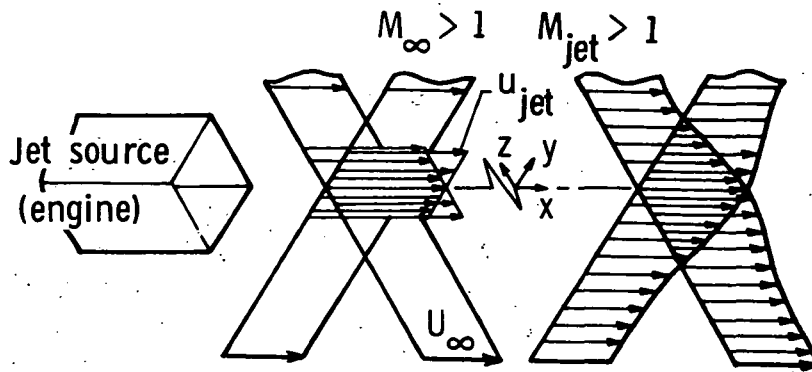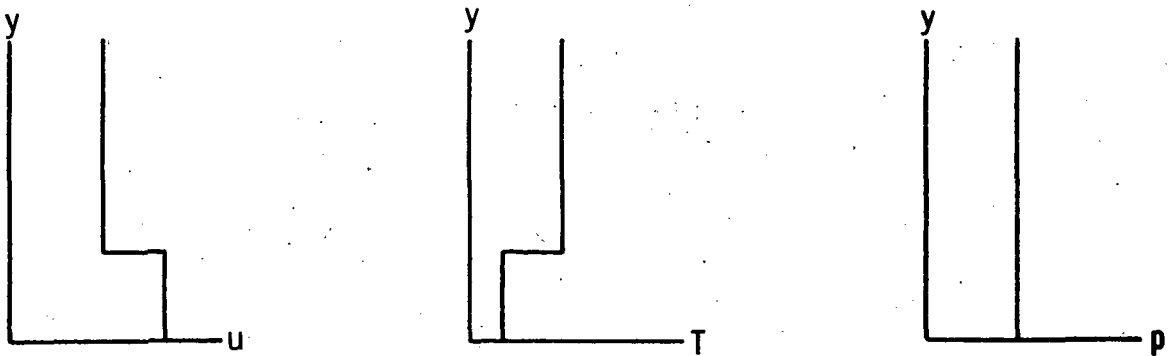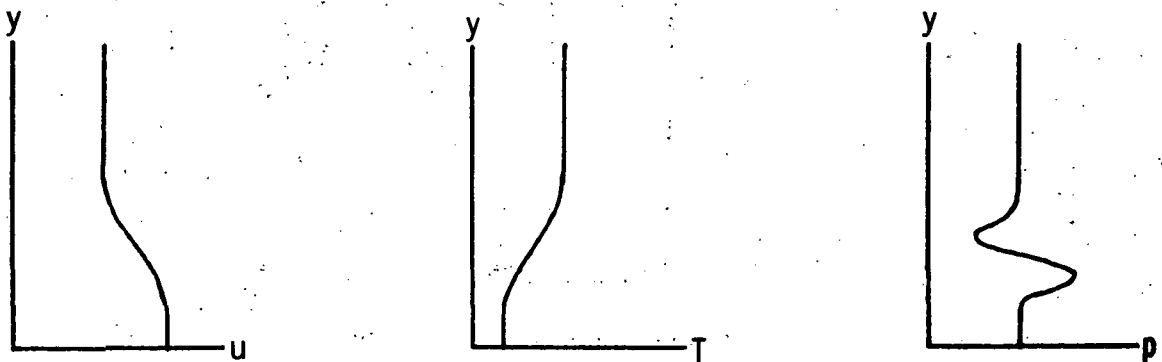
Figure 3.- Conceptual model of three-dimensional supersonic jet flow.

(a) Profiles at $x = 0$.

(b) Profiles downstream of initial plane.

Figure 4.- Initial x-behavior of solution profiles.

$$\delta u = 0 \quad \therefore \quad u_2 - u_0 = 0$$

$$\delta^2 u = \frac{u_2 - 2u_1 + u_0}{\Delta^2} = 2\frac{(u_2 - u_1)}{\Delta^2}$$

• • •3 • •

• • •2 • •

————•————•————•1————•————•————

•0
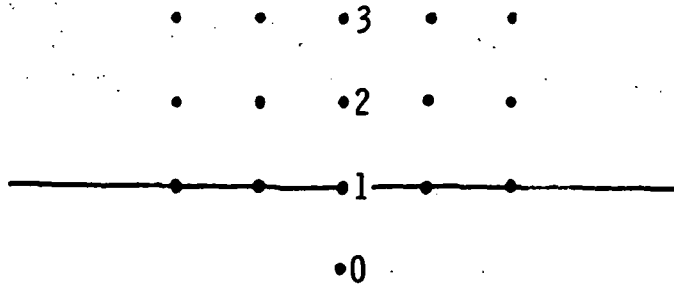
Figure 5. - Differencing used on a boundary.
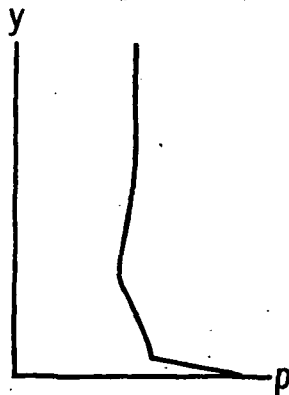
Figure 6. - Qualitative pressure behavior attributed to boundary differencing.
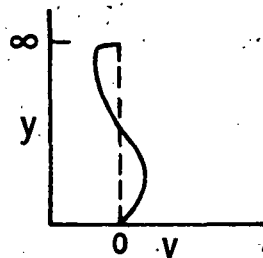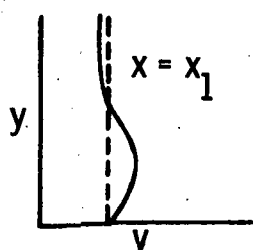
Figure 7.- Crossflow profiles when
free-stream conditions imposed.
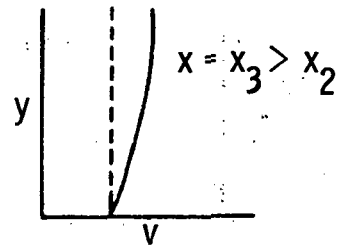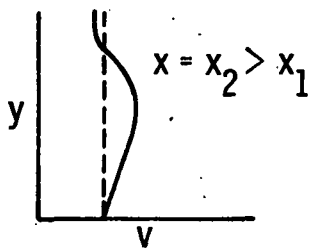
Figure 8.- Crossflow profiles when free-stream conditions extrapolated.
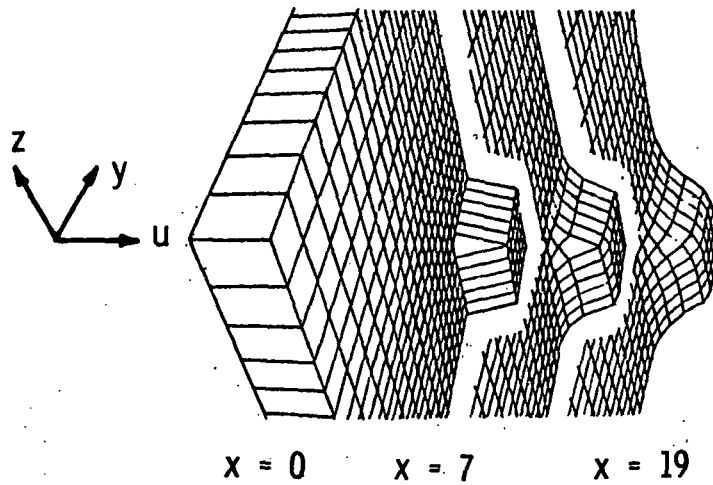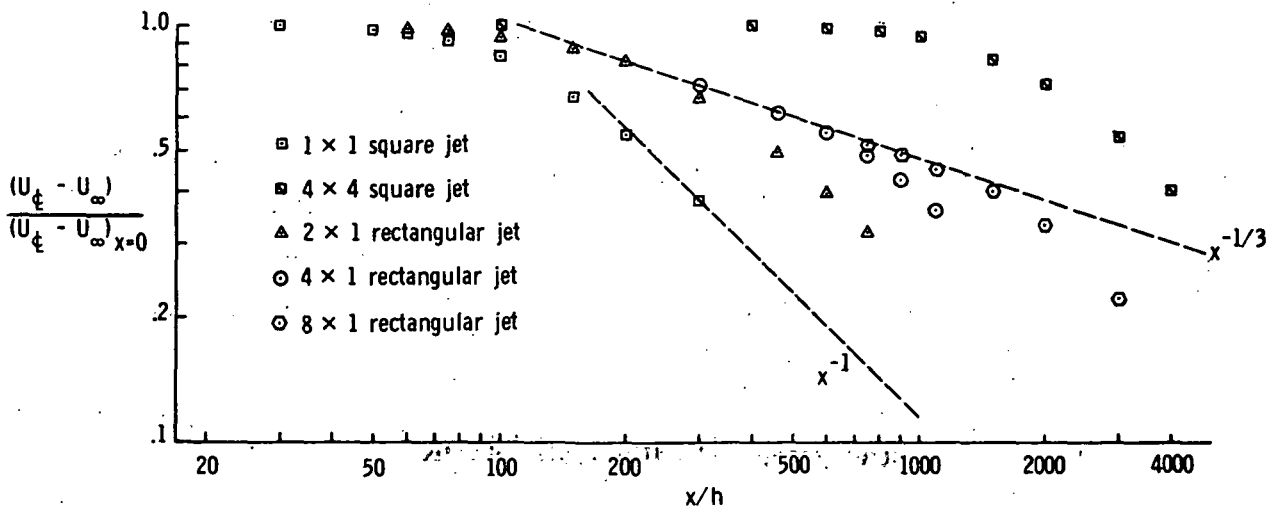
Figure 9.- Computed velocity profiles at various stations.

Figure 10.- Centerline velocity decay for three-dimensional jets.